Chromosome 3p loss of heterozygosity is associated with a unique metabolic network in clear cell renal carcinoma

Francesco Gatto, Intawat Nookaew, and Jens Nielsen[1]

Department of Chemical and Biological Engineering, Chalmers University of Technology, 41296 Göteborg, Sweden

Edited by Robert Langer, Massachusetts Institute of Technology, Cambridge, MA, and approved January 24, 2014 (received for review October 11, 2013)

Several common oncogenic pathways have been implicated in the emergence of renowned metabolic features in cancer, which in turn are deemed essential for cancer proliferation and survival. However, the extent to which different cancers coordinate their metabolism to meet these requirements is largely unexplored. Here we show that even in the heterogeneity of metabolic regulation a distinct signature encompassed most cancers. On the other hand, clear cell renal cell carcinoma (ccRCC) strongly deviated in terms of metabolic gene expression changes, showing widespread down-regulation. We observed a metabolic shift that associates differential regulation of enzymes in one-carbon metabolism with high tumor stage and poor clinical outcome. A significant yet limited set of metabolic genes that explained the partial divergence of ccRCC metabolism correlated with loss of von Hippel-Lindau tumor suppressor (*VHL*) and a potential activation of signal transducer and activator of transcription 1. Further network-dependent analyses revealed unique defects in nucleotide, one-carbon, and glycerophospholipid metabolism at the transcript and protein level, which contrasts findings in other tumors. Notably, this behavior is recapitulated by recurrent loss of heterozygosity in multiple metabolic genes adjacent to *VHL*. This study therefore shows how loss of heterozygosity, hallmarked by *VHL* deletion in ccRCC, may uniquely shape tumor metabolism.

cancer metabolism | systems biology | genome-scale metabolic modeling | renal cancer

There is now widespread consensus that diversion of metabolism is among the most distinguished cancer phenotypes, and it is often postulated to characterize virtually all forms of cancer (1, 2). Indeed, many common oncogenic signaling pathways have been implicated in the emergence of specific metabolic features in cancer cells that have been associated with both survival and sustained abnormal proliferation rate (2–5). However, only a fraction of the metabolic reactions potentially occurring in a generic human cell are typically involved in such processes. Only recently a systemic study using transcriptional regulation has attempted to rule out the possibility that other metabolic processes in the network may achieve equal importance in cancer cells (6), and the idea that all cancer cells display a unique metabolic phenotype has spurred disputes that mainly highlighted a lack of comprehensive evidence (7). Taken together, we contend that only a systems perspective may help to elucidate the extent to which different cancer cells coordinate their metabolic activity.

In this context, systems biology approaches have been demonstrated to lead to the identification of altered metabolic processes in disease development with regard to those disorders that are driven or accompanied by metabolic reprogramming, including cancer (8–11). To this end, the reconstruction of genome-scale metabolic models (GEMs) is instrumental to knit high-throughput data into the metabolic network topology. Such integrative and network-dependent analysis enables prediction of how systems-level perturbations are translated into alterations in distinct and biologically meaningful modules and, at the same time, elucidation of genotype–phenotype relationships (12).

Results

Distinct Changes in Metabolic Gene and Protein Expression in Tumors. Until recently (6, 13, 14) it has been largely overlooked (*i*) the extent to which the metabolic phenotype is dissimilar with respect to healthy cells, and (*ii*) the extent to which it affects the complete metabolic network. We therefore used a GEM of the human cell and integrated high-dimension datasets of omics data, from both tumor-adjacent normal and cancer tissues. GEMs are models that account for all known reactions and matched metabolites in a cell and include the current knowledge for gene–protein reaction associations for each reaction. Here we used the human metabolic reaction (HMR) model, which comprises 7,943 reactions, 3,158 unique metabolites across eight compartments, and 3,674 genes and represents the most comprehensive compilation of human metabolic reactions (15). As for the omics data, we focused on RNAseq gene expression profiles and immunohistochemical proteomics. For cancer samples, we retrieved 539 transcriptomes and 25 proteomes, whereas for tumor-adjacent normal samples we retrieved 257 transcriptomes and 74 proteomes (*SI Appendix*, Table S1 and Dataset S1). We focused to include gene products that overlapped with the list of 3,674 genes in HMR. The HMR coverage was 97% for the transcript profiles in all cancers and tumor-adjacent normal samples. As for the protein profiles, because the protein coverage was heterogeneous across the samples, the HMR coverage was either 18% or 45%, depending on whether both tumor-adjacent normal and cancer samples or only cancer samples were pooled, respectively (*SI Appendix*, *SI Materials and*

Significance

It is suggested that regulation of metabolism is a point of convergence of many different cancer-associated pathways. Here we challenged the validity of this assertion and verified that a transversal metabolic signature in cancer emerges chiefly in the regulation of nucleotide metabolism. However, the most common form of renal cancer deviates from this behavior and presents some defects in its metabolic network not present in the normal kidney and unseen in other tumors. Notably, reduced copy number in key metabolic genes located adjacent to *VHL* (a tumor suppressor gene frequently deleted in this cancer) recapitulates these defects. These results are suggestive that recurrent chromosomal loss of heterozygosity in cancer may uniquely shape the metabolic network.

Author contributions: F.G., I.N., and J.N. designed research; F.G. performed research; F.G. and I.N. analyzed data; and F.G. wrote the paper.

The authors declare no conflict of interest.

This article is a PNAS Direct Submission.

Freely available online through the PNAS open access option.

Data deposition: All cancer genome-scale metabolic models are available through www.metabolicatlas.com.

[1]To whom correspondence should be addressed. E-mail: nielsenj@chalmers.se.

This article contains supporting information online at www.pnas.org/lookup/suppl/doi:10.1073/pnas.1319196111/-/DCSupplemental.

Methods). Even if metabolic-related proteins had lesser coverage, they are fairly representative for most canonical metabolic pathways (*SI Appendix*, Fig. S1).

The degree of similarity in metabolic gene expression between cancer and tumor-adjacent normal samples was assessed using principal component analysis (PCA) and mutual correlation-based hierarchical clustering. First, the similarity in the abundance of all metabolic transcripts across cancer and tumor-adjacent normal samples was evaluated (*SI Appendix*, Figs. S2 and S3). Both PCA and hierarchical clustering show that a group of cancer samples displays a substantial deviation from the general transcriptional pattern of most cancers. However, if these cancer samples are neglected, PCA reveals a consistent transcriptional response in different cancers opposed to tumor-adjacent normal samples, which is independent of cancer type and remarkable because the control samples were obtained adjacent to the tumor (note that the first principal component was neglected because it seems to account for few outliers; *SI Appendix*, Fig. S4). Conversely, hierarchical clustering shows a higher similarity in the gene expression of tissue-specific samples rather than across all cancer-labeled samples (*SI Appendix*, Fig. S3). This shows that cancers undergo a considerable alteration in metabolic gene expression profiles, but they also retain substantial similarity with the regulation of metabolic gene products of their matched tumor-adjacent normal tissue, in accordance with a recent study (6). This led us to speculate that although cancer samples regulate only a subset of metabolic genes upon transformation and preserve the expression of the remaining as in the tissue of origin, this regulation may be consistent and orchestrated across different cancer types. To verify this, PCA and hierarchical clustering were performed for those metabolic genes (~20%) that changed expression at statistical significance and across at least four histological cancer types, thereby subtracting the effect of tissue of origin (Fig. 1*A* and *SI Appendix*, Fig. S5 and Table S2). In both analyses, the distinction between most cancer and tumor-adjacent normal samples becomes apparent. In particular, hierarchical clustering provides clear evidence for the fact that most cancer samples modulate the expression of a distinct group of metabolic transcripts in a similar fashion, regardless of their histological classification. Next, multiple correspondence analysis (MCA) was performed to check whether the conclusions above also hold at the level of protein expression. Accordingly, proteomics data confirm that the expression of metabolic gene products is more similar between cancer samples than to normal tissues, which are distinctly separated (*SI Appendix*, Fig. S6*A*). However, within cancer samples no obvious cluster emerged, perhaps owing to less coverage (*SI Appendix*, Fig. S6*B*). Taken together, these analyses suggest that the transformation entails a partial yet significant remodeling of metabolic regulation, both at the transcript and protein level, which is transversal and to some extent coordinated within the disease phenotype and does not overlap with that of the tumor-adjacent normal tissue.

Deviation of the Transcriptional Program in Clear Cell Renal Carcinoma Metabolism. The above conclusion only holds provided that the cluster of deviating samples is not taken into account. We explored the nature of this cluster by correlating samples with available clinical data, and strikingly, all samples belonging to this cluster share a common histological type [i.e., clear cell renal cell carcinoma (ccRCC)] (*SI Appendix*, Figs. S2 and S3). Furthermore, such an anomalous profile is not attributable to an inherent elevated metabolic activity of the tissue of origin: when PCA was performed on the reduced pool of metabolic genes that significantly changed expression in most cancer types, ccRCC samples still separated clearly (Fig. 1*A* and *SI Appendix*, Fig. S5). Additionally, we noticed that papillary cell renal cell carcinoma samples present in the previous analyses did not overlap in terms of transcript abundance with ccRCC (*SI Appendix*, Fig. S7) and did not correlate with the previously neglected first principal

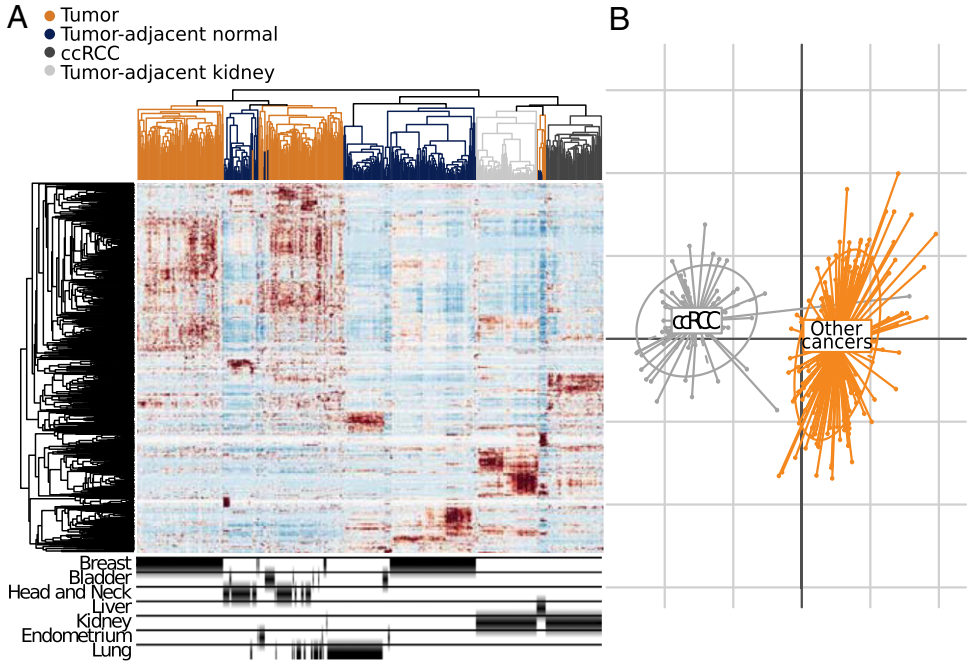

Fig. 1. Clustering analysis of metabolic gene expression profiles for cancer and tumor-adjacent normal samples. (*A*) Hierarchical clustering of absolute metabolic gene expression levels (RPKM) for cancer and tumor-adjacent normal samples, featuring only those genes that significantly changed expression across most cancer types upon transformation, thereby subtracting the effect of the tissue of origin. (*Lower*) Corresponding tissue of origin for each sample in the heatmap above. (*B*) PCA of $\log_2$ metabolic gene expression fold-change vs. matched tumor-adjacent normal samples for ccRCC (gray) and other cancer type samples (orange).

component (*SI Appendix*, Fig. S8). The deviation of ccRCC becomes even more evident when the metabolic gene expression fold-changes (FC) replace the transcript abundance in the PCA, which is suggestive of an opposite direction of regulation compared with other cancer types (Fig. 1*B*). Given that ccRCC samples present a lower and more variable tumor cellularity than the other cancer types in this study (16, 17), we tested the hypothesis that a higher stromal content may be responsible for the apparent outstanding regulation of metabolic gene expression in ccRCC. We inferred scores for tumor purity from gene expression profiles using ESTIMATE (17). These scores showed a moderated increase of infiltrating cells in ccRCC samples compared with others (*SI Appendix*, Fig. S9). However, when each metabolic gene expression fold-change value was adjusted using a simple linear regression on the stromal score for a given sample, we still observed a distinct separation of ccRCC from the other cancer types (*SI Appendix*, Fig. S10). These results suggest that unique patterns of regulation are rewiring ccRCC metabolism, which are markedly distinct from any other cancer in this study and that are not utterly ascribable to the tissue of origin or to the purity of the tumor. Indeed, the comprehensive molecular characterization of ccRCC that produced the data used in this study highlighted a considerable relationship between glycolytic metabolism and overall survival (16). However, the extent to which a shift toward a "Warburg effect"-like state may inherently explain the here-reported deviation of ccRCC metabolic regulation is questionable. Indeed, aerobic glycolysis is a hallmark reported in other different cancer types. Moreover, the number of regulated genes involved in this metabolic process (~40 as reported in ref. 16) is relatively low compared with the number of metabolic genes that clustered ccRCC distant from the other cancer types. These considerations hinted to us that other pathways may be strongly and uniquely regulated in ccRCC. Therefore, we computed for each cancer type the differential gene expression fold-changes compared with tumor-adjacent matched normal samples. We found that 2,539 metabolic genes are significantly regulated in ccRCC vs. tumor-adjacent kidney ($P < 0.05$), of which 329 genes are substantially up-regulated ($\log_2$FC ≥ 1) and 551 down-regulated ($\log_2$FC ≤ -1). This shows that there is a major disproportion toward down-regulation of metabolic genes in ccRCC. To test whether metabolic down-regulation is a common feature across different cancer types upon transformation, the actual discrete adjusted fold-change distribution in the population of ccRCC samples was compared with the population of the remaining cancer samples, and the former tend to have lower values ($P < 10^{-15}$, Mann-Whitney *U* test; *SI Appendix*, Fig. S11). We also observed that the adjustment for the stromal score corrects for an overestimation in terms of down-regulation. Additionally, the empirical cumulative distribution of adjusted fold-changes in the population of ccRCC samples was compared with the population of the remaining cancer samples. Again, we confirmed that there is a significant shift toward down-regulation in ccRCC with respect to the other cancer samples ($P < 10^{-15}$, Kolmogorov-Smirnov test; *SI Appendix*, Fig. S12). On the other hand, when the former test was repeated binning the remaining cancer samples according to their cancer type, endometrial cancer samples also showed a similar tendency (*SI Appendix*, Fig. S13). Taken together, these results are suggestive of widespread repression of metabolic gene expression in ccRCC, which in part explains the deviation observed above.

ccRCC Uniquely Regulates Nucleotide, Glycerolipid, and One-Carbon Metabolism Compared with Any Other Cancer Type, the Latter Being Implicated in Poor Prognosis. Next we sought to characterize the impact of a ccRCC divergent transcriptional program on metabolism as opposed to other cancer types. First, we checked in each PCA whether we could identify a set of relevant loadings responsible for the separation of ccRCC samples from the rest (i.e., the metabolic transcripts with the highest eigenvalues in each principal component—that is, highly associated with a separation on that component). However, neither in the PCA clustering on transcript abundance (*SI Appendix*, Fig. S14) nor in the PCA clustering on direction of gene expression regulation (*SI Appendix*, Fig. S15) could a well-defined set of genes be found. Therefore, we used network-dependent analyses to identify how such a unique program of transcriptional regulation diversely affected metabolism of ccRCC samples. For each of the cancer types we identified reporter metabolites and pathways (18) using our multiple gene-set analysis method (19) (Fig. 2 and *SI Appendix*, Fig. S16). As expected, in ccRCC diverse areas of the metabolic network were either uniquely regulated or not regulated compared with other cancer types, although an ostensible heterogeneity can be viewed across all cancer types (*SI Appendix*, *SI Text*). Among these, nucleotide metabolism and alanine, aspartate, and glutamate metabolism, which were generally found up-regulated in most cancer types, were not significantly altered in ccRCC. On the other hand, the metabolism of other amino acids (namely valine, leucine, isoleucine, cysteine, methionine, glycine, serine, and threonine) was significantly down-regulated only in ccRCC, as much as was the tricarboxylic acid (TCA) cycle and enzymes that participate in the metabolism of ubiquinone and ubiquinol (*SI Appendix*, Fig. S16), intermediates in the electron transport chain (ETC). Finally, we report unique changes in the metabolism of long-chain fatty acids and lactate (*SI Appendix*, Figs. S17 and S18).

Moreover, we noticed that 1,504 genes that showed statistical significance in patientwise expression fold-change across all cancer vs. matched normal samples ($P < 0.05$, rank–product test, Bonferroni correction) did not display any remarkable change in expression level when averaging in the pool of ccRCC samples. Unsupervised hierarchical clustering of patient-specific metabolic gene expression profiles featuring this set of genes revealed two different clusters with opposite regulatory directions (Fig. 3*A*). Interestingly, these clusters correlate with patients' tumor stage ($P = 0.041$, Pearson χ^2 test; Fig. 3*B*). Kaplan-Meier survival plots and log–rank tests were used to assess the differences in overall survival, and accordingly, the high tumor stage cluster is a predictor for poor prognosis ($P = 0.012$, log–rank test; Fig. 3*C*). Therefore, we sought to verify whether an advanced tumor stage drives per se a different transcriptional regulation of metabolism, as recently suggested (16). To test this, 170 metabolic genes that have significantly changed expression between high tumor stage (stage III to IV) and low tumor stage (stage I to II) samples ($P < 0.05$, Wilcoxon rank-sum test) were featured to cluster samples in a supervised fashion. Contrary to the premises, the two clusters that emerged from the analysis had a weaker association in relation to the tumor stage ($P = 0.1554$; *SI Appendix*, Fig. S19) but a comparable power to predict poor prognosis ($P = 0.025$) (Fig. 3*C*). In both scenarios, the curves strikingly superimpose with the survival plots based on the sole tumor stage information (high vs. low tumor stage; Fig. 3*C*), therefore suggesting a metabolic gene expression profile that is shaped after disease progression. To identify novel metabolic functions affected by the differential program of metabolic regulation between the two clusters, we used the reporter metabolite algorithm (18) (*SI Appendix*, Fig. S20). The analysis unveiled some unreported changes (*SI Appendix*, *SI Text*). Among these, we focused on dimethylglycine, a metabolite that belongs to one-carbon metabolism. Dimethylglycine is synthesized from betaine and subsequently converted into glycine (Fig. 3*D*). Most enzyme-coding genes that are uniquely attributable to this pathway display a significant difference in expression regulation between the low and high tumor stage cluster, especially betaine–homocysteine S-methyltransferase 1 (*BHMT*) and 2 (*BHMT2*) whose expression reverse direction completely (*SI Appendix*,

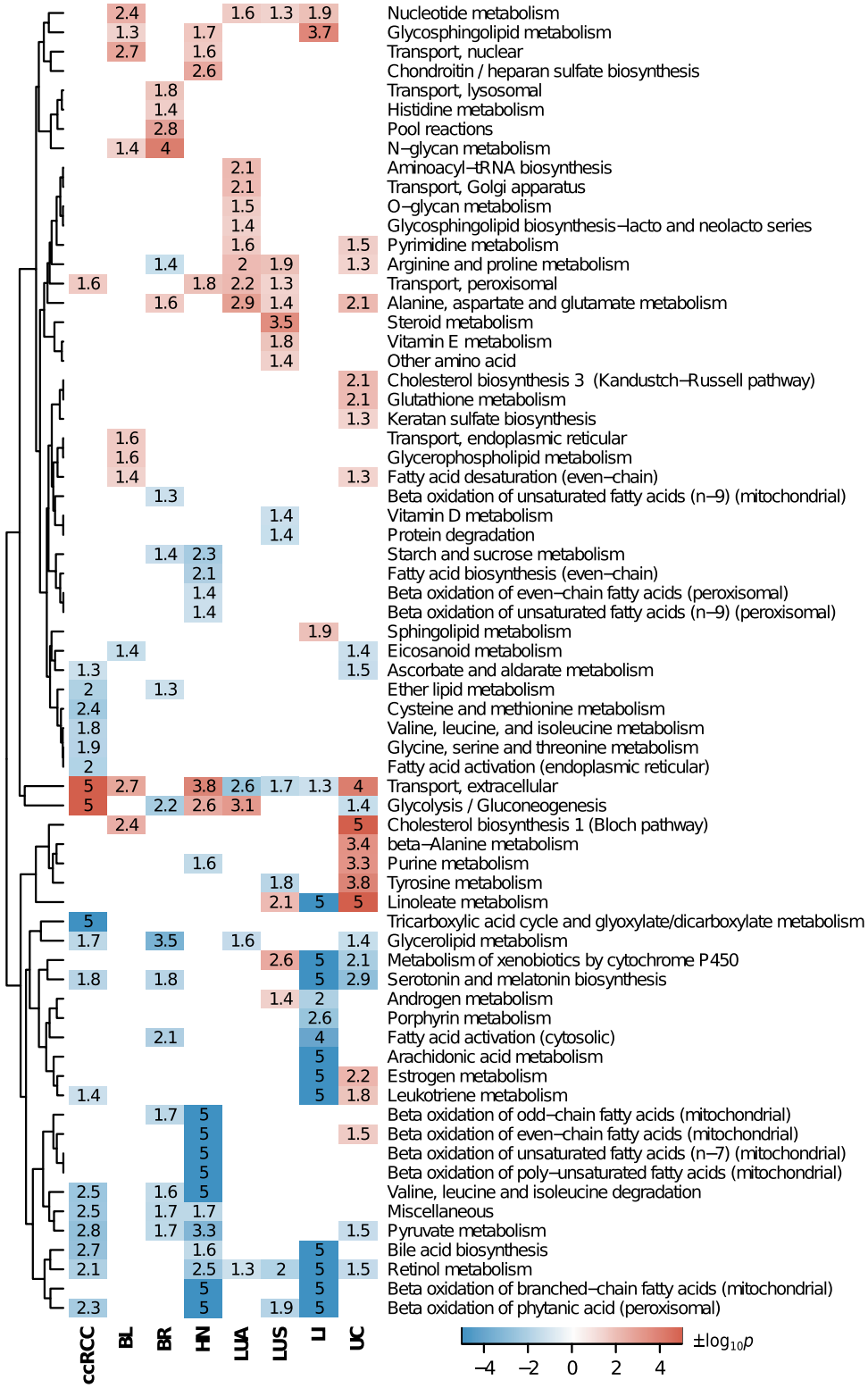

Fig. 2. Reporter canonical metabolic pathways in each cancer type according to significant changes in metabolic gene expression vs. matched tumor-adjacent normal tissues. Each box shows the $\log_{10} P$ value of the gene set representing a pathway in a certain cancer type, and the color indicates the overall direction of gene expression regulation for the gene set (red, up; blue, down). BL, bladder urothelial carcinoma; BR, breast invasive carcinoma; HN, head and neck squamous cell carcinoma; LUA, lung adenocarcinoma; LUS, lung squamous cell carcinoma; LI, liver hepatocellular Ccarcinoma; UC, uterine corpus endometrioid carcinoma.

Fig. S21). These results suggest an unanticipated role for betaine in ccRCC malignancy, which may parallel DNA hypermethylation frequency recently associated with an advanced stage and grade of this tumor (16), given the established role of betaine as a modulator of one-carbon metabolism and homocysteine levels through *BHMT* (20).

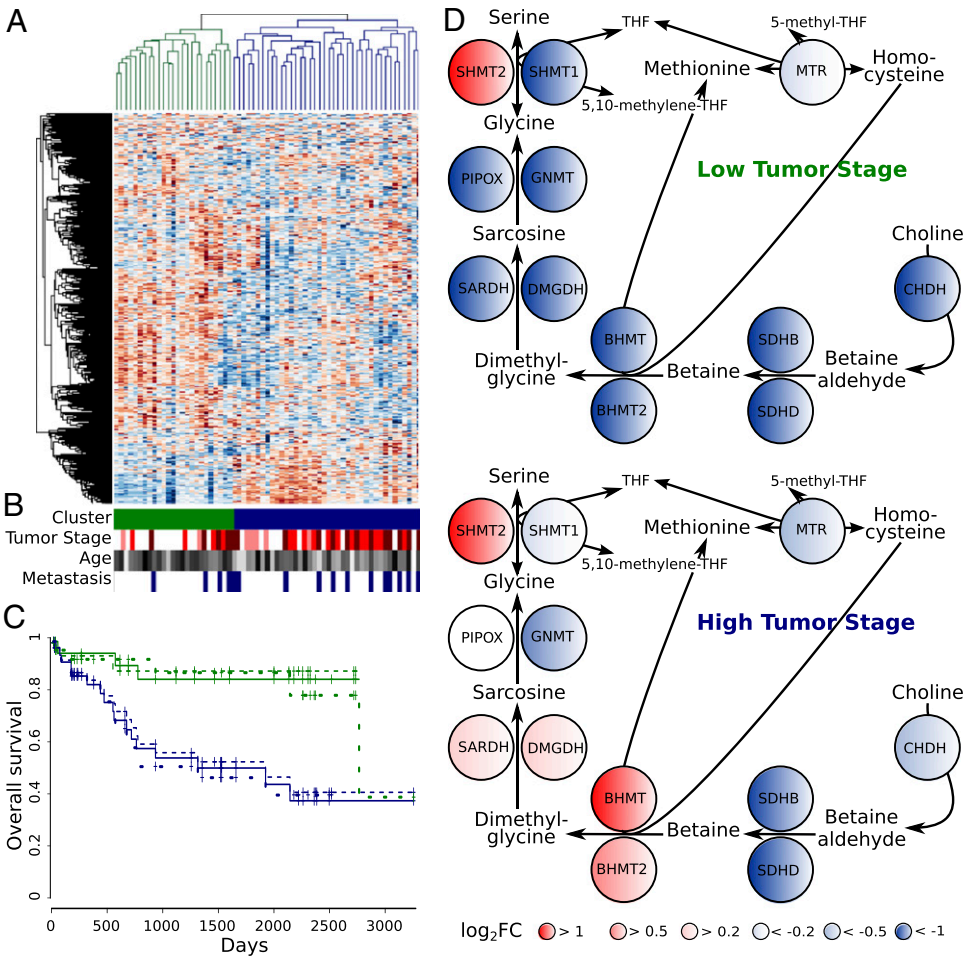

Fig. 3. Metabolic gene expression profiles distinguish two cluster of differential regulation in ccRCC that implicate a role of one-carbon metabolism in the malignancy. (*A*) Unsupervised hierarchical clustering of ccRCC $\log_2$ gene expression fold-changes vs. matched tumor-adjacent normal samples featuring the set of 1,504 metabolic genes significantly different across all $\log_2$ gene expression fold-changes in cancer vs. matched tumor-adjacent normal samples. (*B*) Clinical data for each ccRCC sample as ordered by the hierarchical clustering in *A*. Tumor stage ranges from stage 1 (white) to stage 4 (dark red); age is represented by a gray-scale in which the lowest value is 38 y and highest 90 y; metastatic tumors are depicted in blue. (*C*) Kaplan-Meier survival curves for the two clusters in *A* (solid line), for the two clusters in *SI Appendix*, Fig. S19 defined when featuring significantly changed genes between the pool of high tumor stage and low tumor stage samples (short dashed line), and for the two groups of samples solely identified by a high or low tumor stage (long dashed line). Blue and green lines refer to high and low tumor stage, respectively. (*D*) Gene expression regulation of enzymes involved in choline degradation to glycine in the two clusters in *A*.

Upon Transformation, the ccRCC Metabolic Network Features Widespread Loss of Function in Nucleotide, Glycerolipid, and One-Carbon Metabolism, in Contrast to Any Other Tumors. Because transcriptional regulation in ccRCC is suggestive of diffuse down-regulation of key metabolic functions, we evaluated whether the topology of its metabolic network reflected these premises. Therefore, we generated a cancer cell type-specific GEM based on protein evidence, using the INIT algorithm (21). Using the generic human model HMR as a template, INIT reduces the network according to proteomics evidence covering 15,156 proteins across at least 10 renal carcinomas (>70% are clear cell). Of 15,156 protein-coding genes, 2,482 could be mapped to HMR, and the reconstructed GEM, *iRenalCancer1410*, accounts for 3,913 reactions, 2,053 metabolites, and 1,410 genes, which means a reduction of 4,318 reactions (−53%) and 2,264 genes (−62%) from the generic human metabolic model, mostly due to no or little evidence for the encoded protein in most renal cancer samples (*SI Appendix*, Fig. S22*A*). To assess which losses of metabolic function are attributable to the transformation, we compared *iRenalCancer1410* with a published metabolic model of the kidney cell in tubules (21), accounting for 4,812 reactions, 2,268 metabolites, and 2,240 genes (*SI Appendix*, Fig. S22*B*). The comparison evidenced two interesting points. First, upon transformation, the renal cancer metabolic network shrinks with a reduction by approximately 20% of the number of reactions and a reduction of more than 35% of the number of associated genes, which clearly demonstrates a significant loss of metabolic functions. Second, 852 metabolic genes that are present at the protein level in the normal kidney cell are lost in the transformed cell. These genes mainly belong to the metabolism of nucleotides, glycerolipids, glycerophospholipids, glycosphingolipids, oxidative phosphorylation, and inositol metabolism, among others (Fig. 4*A*). Conversely, 22 metabolic genes present only the renal cancer network are associated with oxidoreductases in the endoplasmic reticulum. To validate whether these metabolic perturbations occurring during the transformation can be uniquely attributed to renal cancer and therefore provide insights on the deviating pattern of ccRCC metabolic regulation, we reconstructed cancer cell type-specific metabolic models for four additional cancer types (breast, lung, liver, and bladder) using the same procedure described above. In line with the previous results that highlighted a pronounced shift toward metabolic down-regulation in ccRCC

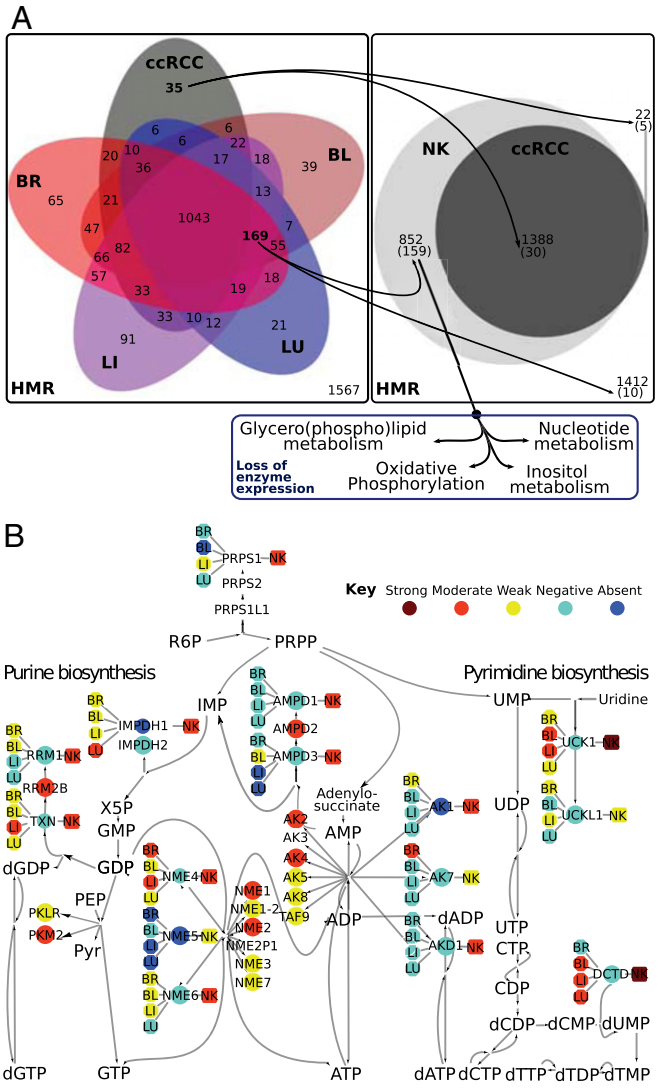

Fig. 4. Reconstruction and comparison of ccRCC-specific GEM (*iRenalCancer1410*) against other cancer-type GEMs and the normal kidney cell in tubules GEM. (*A*) Venn diagram for the metabolic genes present in *iRenalCancer1410* compared with other reconstructed GEMs (cancers, *Left*, kidney cell in tubules, *Right*). Metabolic genes absent in *iRenalCancer1410* but present both in the kidney cell in tubules GEM and other cancer type GEMs were used to enrich canonical pathways. (*B*) Nucleotide metabolism featuring the staining level of proteins taken from HPA for different tissues (*Center*: ccRCC; *Left*: BR, breast cancer; BL, bladder cancer; LI, liver cancer; LU, lung cancer; *Right*: NK, kidney cell in tubules).

compared with any other tumor, the metabolic network reconstruction of *iRenalCancer1410* resulted in a substantially smaller model than in any of the other cancers. Moreover, the comparison of each of the four metabolic networks against *iRenalCancer1410* revealed that 169 metabolic genes were present in all cancer models except for the renal cancer model, more than for any other cancer (on average, 41 ± 28 metabolic genes are lost in a model compared with the rest; Fig. 4*A*). Strikingly, 159 of these genes are also present in the normal kidney cell metabolic network, therefore confirming that the above-observed metabolic perturbations in ccRCC are unique. As a consequence, key enzymes are missing in the metabolism of glycerophospholipids, inositol, and one-carbon, as well as oxidative phosphorylation (Fig. 4*A* and *SI Appendix*, Fig. S23). Additionally, nucleotide metabolism is severely compromised, spanning both de novo biosynthesis, which is generally up-regulated in cancer (6), and successive degradation of nucleosides (Fig. 4*B*). In particular, we observe that absence of inosine 5′-monophosphate dehydrogenase 1 (IMPDH1) and 2 (IMPDH2), which commit IMP to initiate guanosine synthesis; RRM1 and TXN, which catalyze the synthesis of deoxyribonucleotides from the corresponding ribonucleotides; NME/NM23 family member 5 (NME5), NME/NM23 nucleoside diphosphate kinase 4 (NME4) and 6 (NME6), which are involved in nucleoside triphosphates biosynthesis from nucleoside diphosphates; and several enzymes in the 5′(3′)-deoxyribonucleotidase family, which dephosphorylates different deoxyribonucleotides. Taken together, a widespread repression of protein expression clearly limits the redundancy of genes in key metabolic pathways (most importantly nucleotide metabolism), a fact undetected in any other cancer type.

Divergence of ccRCC Metabolic Regulation Can Be Ascribed to Loss of Heterozygosity in Key Metabolic Genes Adjacent to von Hippel-Lindau Tumor Suppressor After Its Deletion. The divergence of ccRCC metabolic regulation compared with any other tumor and normal kidney is apparent both in the transcriptional regulation and its metabolic network. On one hand, the analysis of transcriptional regulation revealed that even though each type of cancer in this study displayed a complex and heterogeneous pattern of metabolic regulation in different pathways, ccRCC features a unique tendency to generally down-regulate large parts of metabolism. Only ccRCC strongly represses expression of cysteine and methionine metabolism (part of one-carbon metabolism), branched-amino acids metabolism, the metabolism of glycine, serine, and threonine, the TCA cycle and the ETC, as well as glycerolipid metabolism (with emphasis on fatty acid elongation). Additionally, whereas most tumors up-regulate nucleotide metabolism and the metabolism of alanine, aspartate, and glutamate, ccRCC shows a mixed pattern of regulation that results in both overexpressed and repressed genes in these pathways. On the other hand, the analysis of the metabolic network uncovered that ccRCC relies on a relatively small network, which features loss of gene redundancy in key metabolic pathways (e.g., oxidative phosphorylation and nucleotide, inositol, one-carbon, and glycerolipid metabolism) otherwise unaffected in any other cancer or in the normal kidney. Therefore, we sought to characterize the possible causes underlying the above-described metabolic features that render ccRCC different from all of the other cancer types upon transformation (Fig. 5).

First we considered the genetic background of ccRCC. Sporadic ccRCC (which represents 75% of all renal carcinomas) is generally characterized by mutations in the *VHL* tumor suppressor gene (16, 22). Deletion of Von Hippel-Lindau tumor suppressor (*VHL*) results in the stabilization of the hypoxia-inducible transcription factor (HIF) under normoxic conditions and thus entails a profound rewiring of mammalian oxygen-sensing pathways (23). Therefore, we tested the hypothesis that loss of *VHL* is one of the possible causes for the unique metabolic reprogramming of ccRCC. First, copy number variants (CNVs) for 62 ccRCC samples used in the PCA were checked in the region of *VHL*, and in 90% (56 of 62) of the samples the *VHL* gene locus was found consistently deleted, as opposed to matched tumor-adjacent normal samples (*SI Appendix*, Fig. S24). In addition, 52% of these samples (32 of 62) harbored a *VHL* mutation that mostly results in the deactivation of the corresponding protein (*SI Appendix*, Fig. S24). Second, the metabolic gene expression changes for each examined cancer type vs. matched normal tissues were correlated with an analogous comparison between two isogenic ccRCC cell lines (786-O), in which one of the cell lines is a *VHL* mutant with a frameshift deletion, whereas the second had *VHL* reintroduced (24). By comparing the *VHL*-deficient cell line against the *VHL*-reintroduced cell line, 1,339 genes were

found significantly regulated, of which 290 are metabolic ($P < 0.05$, 119 up-regulated, 171 down-regulated). Among all of the cancer types analyzed, only the direction changes in metabolic gene expression coming from ccRCC samples correlated with the above pattern of transcriptional regulation ($P < 0.05$; *SI Appendix*, Fig. S25). The correlation is even stronger when a more stringent significance level is used ($P < 0.01$; *SI Appendix*, Fig. S26). Despite the limited number of genes differentially regulated in the *VHL*-deficient cell line, the amount of metabolic genes coregulated with ccRCC (228) was found to be overrepresented ($P < 10^{-4}$, Fisher's exact test), in particular the up-regulated ones ($P < 10^{-4}$; *SI Appendix*, Fig. S27). Such genes are not exclusively ascribable to kidney or renal carcinoma, as revealed by functional clustering based on tissue expression data (*SI Appendix*, Table S3). These results were successfully replicated using an analogous yet independent dataset (25) (*SI Appendix*, Fig. S25). The analysis of these data indicates that in ccRCC *VHL* loss is indeed associated with the regulation of a significant portion of metabolic genes, whereas such association could not be recapitulated in any other cancer type. We therefore explored the metabolic functions affected by expression changes in the 228 genes regulated by loss of *VHL* that are associated with ccRCC. To this end, reporter pathways were computed as described above. Only three pathways were shown to be significantly regulated in a consistent direction by this set of genes, namely alanine, aspartate, and glutamate metabolism, valine, leucine, and isoleucine metabolism, and fatty acid elongation (*SI Appendix*, Fig. S28). In all three cases, gene expression was shifted toward down-regulation. Therefore, loss of *VHL* alone may explain why these pathways are repressed or mixed regulated only in ccRCC and not in the other tumors (Fig. 2 and *SI Appendix*, Fig. S16). Given *VHL* involvement in oxygen sensing, we also tested whether pseudohypoxia induced by *VHL* inactivation may drive per se a divergent transcriptional response with respect to environmental hypoxia seen in most tumors and the normal kidney (26, 27), but no such correlation could be found (*SI Appendix*, *SI Text* and Fig. S29).

Apart from *VHL* loss-mediated stabilization of HIF, other transcription factors may be triggered only in ccRCC, thus shedding light on the other differentially regulated metabolic functions. Hence, metabolic gene expression changes were used in our multiple gene-set analysis method to identify reporter transcription factors in each cancer type (*SI Appendix*, *SI Text* and Fig. S30). Notably, signal transducer and activator of transcription 1 (STAT1), an anticarcinogenic transcription factor (28), is deemed associated only to ccRCC as it regulates many of the up-regulated metabolic genes. Indeed, the STAT1 gene set comprises 4,381 genes, and 264 of them are metabolic genes that were significantly overexpressed in ccRCC ($P < 0.01$). Surprisingly, these genes were found to relate to inositol and nucleotide metabolism, among others (*SI Appendix*, Table S4), even though the above analysis of the ccRCC metabolic network rather suggested that these pathways were compromised. However, a detailed review unveiled that these metabolic genes are complementary to the ones found not expressed at the protein level in ccRCC. For instance, the nucleotide metabolism-related genes, namely *NME1*, *NME1-NME2*, *NME2*, and *PKM2*, are all part of ccRCC metabolic network and compensate the lack of expression of *NME4*, *NME5*, and *NME6* at the protein level (Fig. 4*B*). The same can be concluded for inositol metabolism, in which induction of *PIK3C2B*, *PIK3R3*, and *PIK3CD* contrasts with low to null expression of *PI4KB*, *PI4K2A*, and *PI4K2B* (*SI Appendix*, Fig. S23). Therefore, if STAT1 was indeed activated in ccRCC, then together with *VHL* loss it can explain most of the metabolic features that distinguished ccRCC from any other cancer in this study.

The mechanisms for other features unique to ccRCC, such as loss of gene redundancy in nucleotide and glycerolipid metabolism as well as down-regulation of one-carbon metabolism, still remained unsettled. Although this may be seen as part of a general shift toward down-regulation that has related to multistep cancer transformation and suggestive of dedifferentiation (29), we had previously ruled out a compelling role of the tissue of origin in ccRCC metabolic reprogramming (Fig. 1*A* and *SI Appendix*, Fig. S5). We therefore sought to identify whether other genetic alterations may be implicated. Thus we analyzed 488 ccRCC samples and as many matched normal samples for which CNVs were scanned using Affymetrix Genome-Wide SNP Array 6.0 (*SI Appendix*, Dataset S2). We restricted our analysis to those gene loci that overlap with the metabolic genes in HMR and that displayed appreciable mean segment amplitude with respect to the baseline ($>\pm 0.15$) across at least 50% of the samples. Furthermore, all mean segments amplitudes that were not found to be statistically different in the pool of ccRCC samples against tumor-adjacent normal samples were discarded ($P < 0.01$, Wilcoxon rank–sum test). In total, 108 metabolic genes were deemed to be recurrently deleted (107) or amplified (1) in ccRCC (*SI Appendix*, Fig. S31). Transcript and protein abundance for each of these genes were checked in ccRCC against tumor-adjacent normal samples, and 14 genes displayed a consistent trend with the presumptive CNV (*SI Appendix*, Fig. S32 and Table S5). Among these, abhydrolase domain containing 5 (*ABDH5*), choline dehydrogenase (*CHDH*), glycerol-3-phosphate dehydrogenase 1-like (*GPD1L*), *IMPDH2*, and pyruvate dehydrogenase beta (*PDHB*) are located within 3p14.3 and 3p22.3, a region that display significant decrease in gene copy number in the range of 75–81% of samples (Table 1). Reduced copy number for all these metabolic genes may share the same mechanism that induces early loss of *VHL* in ccRCC, being *VHL* located at 3p25.3. Only *PDHB* is known to be indirectly inhibited after *VHL* loss, via HIF-dependent expression of PDHK1, a PDH complex inhibitor (30). Remarkably, these deletions explain many defects previously unveiled in ccRCC metabolic regulation: ABHD5 and GPD1L are involved in glycerophospholipid metabolism; CHDH is implicated in one-carbon metabolism; PDHB commits pyruvate in the TCA cycle; and IMPDH2 is a key step in purine biosynthesis. Taken together, these results are suggestive of a multistep model for ccRCC metabolic reprogramming (Fig. 5): first, *VHL* loss in ccRCC ini-

Table 1. Potentially deleted genes according to copy number (CNV), transcript level (abundance [reads per kilobase per million reads (RPKM)] and regulation [log_2FC]), and median protein staining level in malignant and healthy renal tissue

Gene	Gene locus	Mean CNV amplitude	CNV frequency (%)	RPKM	log_2FC	Median staining renal cancers	Staining kidney cells in tubules	Enzymatic activity
ABHD5	3p21.31	−0.236	81.15	2.69	−0.94	Negative	Moderate	1-acylglycerol-3-phosphate O-acyltransferase
CHDH	3p21.1	−0.227	78.28	9.54	−1.05	Negative	Strong	Choline dehydrogenase
GPD1L	3p22.3	−0.234	80.94	4.96	−0.83	Negative	Moderate	Glycerol-3-phosphate dehydrogenase
IMPDH2	3p21.31	−0.236	81.15	8.19	−0.68	Negative	Moderate	IMP dehydrogenase
PDHB	3p14.3	−0.216	74.80	4.35	−1.30	Negative	Strong	Pyruvate dehydrogenase

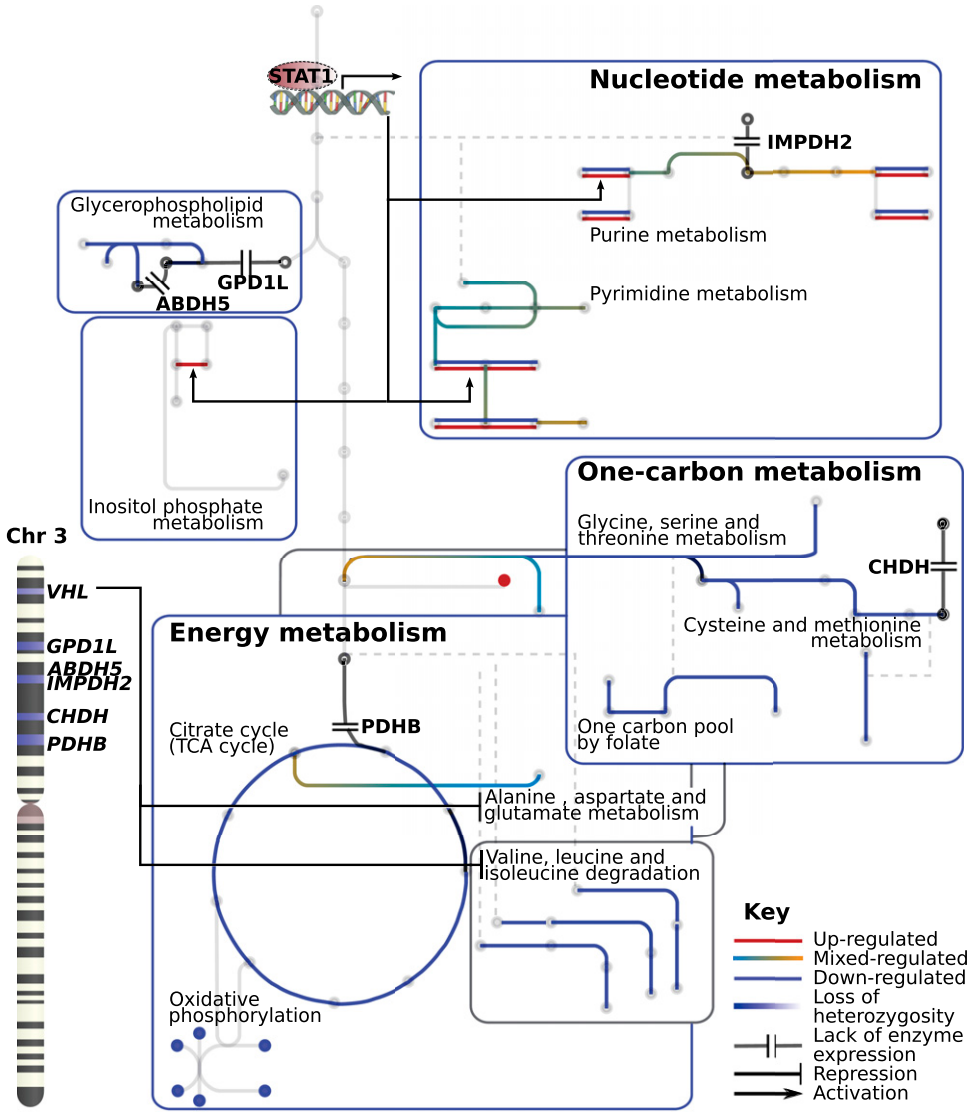

Fig. 5. An overview of the metabolic features unique to ccRCC in the landscape of cancer metabolic regulation. The figure shows reporter pathways (represented by edges; refer to Fig. 2) and metabolites (represented by nodes; refer to *SI Appendix*, Fig. S16) transcriptionally regulated only in ccRCC vs. matched tumor-adjacent normal tissue; and subnetworks (represented by rectangles) that feature lack of gene redundancy only in ccRCC metabolic network (refer to Fig. 4*A*). The mechanisms that contribute to this metabolic phenotype are summarized. First, loss of *VHL* represses expression of metabolic genes in alanine, aspartate, glutamate, and branched-chain amino acids metabolism. Second, potential activation of STAT1 up-regulates redundant genes in nucleotide biosynthesis and inositol metabolism. Third, loss of heterozygosity in metabolic genes adjacent to *VHL* affects several pathways previously identified as down-regulated or deficient only in ccRCC (represented by double bar).

tiates an extensive transcriptional program that also represses peripheral metabolism (e.g., branched-chain amino acids metabolism); then, recurrent loss of heterozygosity in 3p affects several adjacent metabolic genes that implicate reduced redundancy in the ccRCC metabolic network (e.g., impaired purine biosynthesis); finally, transition to malignancy and a possible activation of STAT1 may contribute to trigger adaptive mechanisms (e.g., regulation of one-carbon and nucleotide metabolism).

Discussion

The increasing body of evidence that the same deregulated signaling pathways that lead to the typical malignancy of cancer cells converge in the regulation of cell metabolism has lately gained attention for the possible implications in cancer therapy (31). Moreover, this fact propelled the idea that oncogene-directed metabolic reprogramming is a strict condition to support anabolic growth and meet the metabolic requirements for proliferation in any cancer cell (2, 5). However, the degree to which regulation of such reprogramming is equated across different cancer cells at the systems level has been largely overlooked. In this study, and in remarkable concordance with the work by Hu et al. (6), a systems analysis of the metabolic network revealed that cancer cells orchestrate the expression of metabolic genes in a similar fashion only when it comes to nucleotide, glutamate, and retinol metabolism, while retaining the expression of a substantial portion of metabolic genes unaltered with respect to their tissue of origin. As a proof of concept, it has been recently appreciated that sustained growth signaling via mTORC1, a pathway constitutively active in most human cancers, directly controls de novo pyrimidine biosynthetic flux (32, 33).

The fact that ccRCC has a radically different metabolic regulatory program at the systems level may therefore be important not only for the rational design of therapeutic targets against this particular neoplasm, but also to understand cancer metabolism

in general. Recently a comprehensive characterization of ccRCC unveiled an exceptional regulation of central carbon metabolism, associated with altered promoter methylation patterns and mutations in the PI(3)K/AKT pathway (16). Here we report that peripheral regions of metabolism (e.g., nucleotide, one-carbon, amino acid, and glycerolipid metabolism) are also uniquely affected in ccRCC, and we provide evidence that this divergence of ccRCC metabolic regulation can be ascribed to recurrent loss of heterozygosity. Indeed, in line with the idea that oncogenic pathways are implicated in the regulation of cancer metabolism, we show that loss of *VHL* in the 3p chromosome drives an initial reprogramming that matched exclusively in the case of ccRCC. Accordingly, a recent study that reconstructed a single tumor genetic phylogeny confirmed that *VHL* deletion is the earliest event in ccRCC cancerogenesis (34). Such reprogramming entails down-regulation of branched-chain amino acid metabolism, fatty acid elongation, and alanine, aspartate, and glutamate metabolism, the latter otherwise generally up-regulated in most cancers. Thereafter, loss of heterozygosity in key metabolic genes adjacent to *VHL* compromise nucleotide, one-carbon, and inositol metabolism and glycerolipid biosynthesis. In support of our conclusion, a study specifically aiming to map deletions on 3p besides *VHL* in ccRCC tissue samples revealed extensive loss of heterozygosity in gene loci within the chromosome, with remarkably higher frequency at a late tumor stage (35). Such events therefore imply in ccRCC loss of gene redundancy in a metabolic pathway, namely nucleotide metabolism, which is the most frequently overexpressed in cancer (6). As such, considering its essential role for cancer proliferation, such a finding paves the way for potential synthetic lethality strategies. Intriguingly, ccRCC cells seem to adapt to its defective network by up-regulating alternative pathways, as in the case of betaine, where we find that this adaptation may turn critical for the aggressiveness of the disease. In addition, a potential activation of STAT1 transcription factor was associated only with ccRCC. Such activation would trigger up-regulation of complementary genes in nucleotide and inositol metabolism, explaining the mixed regulation of the former in ccRCC. Although STAT1 activation requires experimental validation, this event may be linked to immune response (28) or to treatment with interferon-α (36). Finally, we considered environmental hypoxia and kidney cell dedifferentation as other potential factors that may contribute to a different metabolic reprogramming in ccRCC, but no compelling role could be demonstrated in either case. In conclusion, there is evidence that ccRCC metabolic regulation is uniquely shaped upon loss of heterozygosity in the 3p chromosome, where VHL, the tumor suppressor gene most commonly associated to ccRCC, is located.

Finally, Hu et al. (6) reported that in the few cases in which nucleotide biosynthesis was not up-regulated in cancer, the overall metabolic gene expression was most down-regulated or not changed. Indeed, here we found that ccRCC displays a significant shift toward metabolic down-regulation, which translated in the smallest metabolic network, and features a compromised nucleotide metabolism. We therefore addressed this discrepancy in ccRCC and propose that loss of heterozygosity may be instrumental in shaping the metabolic topology of these cancer cells. As such, we also believe that these results reinforce the idea that among all other cancers nucleotide biosynthesis is a crucially altered pathway marked with increased activity.

Materials and Methods

Data. RNAseq profiles for primary tumor and matched tumor-adjacent normal tissues were obtained at The Cancer Genome Atlas (TCGA, tcga-data.nci.nih.gov). Immunohistochemical protein profiles were retrieved at the Human Protein Atlas (HPA version 11, www.proteinatlas.org). GEMs for a generic human cell (HMR3674, shortly HMR) and the kidney cell in tubules were downloaded from the Human Metabolic Atlas (www.metabolicatlas.com). Detailed information is given in *SI Appendix, SI Materials and Methods*.

Cluster Analysis. PCA and hierarchical clustering (Pearson correlation metric, average linkage), were performed on the basis of metabolic transcript abundance profiles [measured in reads per kilobase per million reads (RPKM)] or $\log_2$ metabolic gene expression fold-change against matched tumor-adjacent normal samples focusing only on those genes included in HMR. MCA was based on four categorical staining levels (strong, moderate, weak, and negative) for metabolic gene encoded proteins. Detailed information is given in *SI Appendix, SI Materials and Methods*.

Gene-Set Analysis. Multiple gene-set analyses were implemented using PIANO R-package (19), and each gene set was defined as either the set of genes constituting a pathway in HMR (reporter pathway), or as the set of genes that encode for all reactions involving a certain metabolite in HMR (reporter metabolites), or as the set of genes for which a peak was detected in any ChIP-seq experiment, as collected in Cscan (37), targeting a certain transcription factor (reporter transcription factors). For each directionality class (up-, down-, or mixed regulated), the statistical significance returned is the median significance reported by eight gene-set analysis methods. Then, the most significant directionality class is reported. Detailed information is given in *SI Appendix, SI Materials and Methods*.

Statistical Analysis. Details on the statistical tests reported in the text are available in *SI Appendix, SI Materials and Methods*. For gene expression differential analysis, cancer type-wise statistics were computed from empirical Bayes estimation and generalized linear models to fit a negative binomial distribution on the read counts; patient-wise statistics were computed using the rank–product test adjusted using the Bonferroni correction. Detailed information is given in *SI Appendix, SI Materials and Methods*.

Cancer GEMs Reconstruction. The reconstruction of cancer type-specific GEMs was performed for breast, bladder, liver, lung, and renal cancer using the INIT algorithm (21) within the RAVEN Toolbox (38). Scoring for evidence of a reaction to be occurring was based on HPA protein profiles for each cancer type. INIT reconstructs a GEM by maximizing the reaction score while preserving network connectivity and functionality (i.e., the resulting GEM must be able to perform a list of metabolic tasks, including biomass growth). Detailed information is given in *SI Appendix, SI Materials and Methods*. All cancer models are available through www.metabolicatlas.com.

CNV Analysis. SNP arrays for CNV analyses were obtained at TCGA for ccRCC and matched tumor-adjacent normal samples, and segment amplitude across each chromosome was calculated using the GADA R-package (39). Detailed information is given in *SI Appendix, SI Materials and Methods*.

ACKNOWLEDGMENTS. We thank Amir Feizi, Rahul Kumar, Adil Mardinoglu, Natapol Pornputtapong, Kaisa Thorell, Sergio Velasco, Leif Väremo, Rasmus Ågren, and Tobias Österlund for discussion and computational support, and Verena Siewers and Josè Luis Martinez for editing the article. The Cancer Genome Atlas provided access and diffusion of restricted data. The computations were performed on resources provided by the Swedish National Infrastructure for Computing at C3SE. This work was sponsored by the Knut and Alice Wallenberg Foundation and the Chalmers Foundation.

1. Hanahan D, Weinberg RA (2011) Hallmarks of cancer: The next generation. *Cell* 144(5):646–674.
2. Ward PS, Thompson CB (2012) Metabolic reprogramming: A cancer hallmark even Warburg did not anticipate. *Cancer Cell* 21(3):297–308.
3. Schulze A, Harris AL (2012) How cancer metabolism is tuned for proliferation and vulnerable to disruption. *Nature* 491(7424):364–373, and erratum (2012) 494(7435):130.
4. Cairns RA, Harris IS, Mak TW (2011) Regulation of cancer cell metabolism. *Nat Rev Cancer* 11(2):85–95.
5. Vander Heiden MG, Cantley LC, Thompson CB (2009) Understanding the Warburg effect: The metabolic requirements of cell proliferation. *Science* 324(5930):1029–1033.
6. Hu J, et al. (2013) Heterogeneity of tumor-induced gene expression changes in the human metabolic network. *Nat Biotechnol* 31(6):522–529.
7. Moreno-Sánchez R, Rodríguez-Enríquez S, Marín-Hernández A, Saavedra E (2007) Energy metabolism in tumor cells. *FEBS J* 274(6):1393–1418.
8. Mardinoglu A, Gatto F, Nielsen J (2013) Genome-scale modeling of human metabolism—a systems biology approach. *Biotechnol J* 8(9):985–996.
9. Jerby L, Ruppin E (2012) Predicting drug targets and biomarkers of cancer via genome-scale metabolic modeling. *Clin Cancer Res* 18(20):5572–5584.
10. Väremo L, Nookaew I, Nielsen J (2013) Novel insights into obesity and diabetes through genome-scale metabolic modeling. *Front Physiol* 4:92.

11. Lewis NE, Abdel-Haleem AM (2013) The evolution of genome-scale models of cancer metabolism. *Front Physiol* 4:237.
12. Lewis NE, Nagarajan H, Palsson BO (2012) Constraining the metabolic genotype-phenotype relationship using a phylogeny of in silico methods. *Nat Rev Microbiol* 10(4):291–305.
13. Frezza C, et al. (2011) Haem oxygenase is synthetically lethal with the tumour suppressor fumarate hydratase. *Nature* 477(7363):225–228.
14. Folger O, et al. (2011) Predicting selective drug targets in cancer through metabolic networks. *Mol Syst Biol* 7:501.
15. Mardinoglu A, et al. (2013) Integration of clinical data with a genome-scale metabolic model of the human adipocyte. *Mol Syst Biol* 9:649.
16. Creighton CJ, et al. (2013) Comprehensive molecular characterization of clear cell renal cell carcinoma. *Nature* 499(7456):43–49.
17. Yoshihara K, et al. (2013) Inferring tumour purity and stromal and immune cell admixture from expression data. *Nat Commun* 4:2612.
18. Patil KR, Nielsen J (2005) Uncovering transcriptional regulation of metabolism by using metabolic network topology. *Proc Natl Acad Sci USA* 102(8):2685–2689.
19. Väremo L, Nielsen J, Nookaew I (2013) Enriching the gene set analysis of genome-wide data by incorporating directionality of gene expression and combining statistical hypotheses and methods. *Nucleic Acids Res* 41(8):4378–4391.
20. Ueland PM, Holm PI, Hustad S (2005) Betaine: A key modulator of one-carbon metabolism and homocysteine status. *Clin Chem Lab Med* 43(10):1069–1075.
21. Agren R, et al. (2012) Reconstruction of genome-scale active metabolic networks for 69 human cell types and 16 cancer types using INIT. *PLOS Comput Biol* 8(5):e1002518.
22. Cohen HT, McGovern FJ (2005) Renal-cell carcinoma. *N Engl J Med* 353(23):2477–2490.
23. Kim WY, Kaelin WG (2004) Role of VHL gene mutation in human cancer. *J Clin Oncol* 22(24):4991–5004.
24. Vanharanta S, et al. (2013) Epigenetic expansion of VHL-HIF signal output drives multiorgan metastasis in renal cancer. *Nat Med* 19(1):50–56.
25. Papandreou I, Cairns RA, Fontana L, Lim AL, Denko NC (2006) HIF-1 mediates adaptation to hypoxia by actively downregulating mitochondrial oxygen consumption. *Cell Metab* 3(3):187–197.
26. Harris AL (2002) Hypoxia—a key regulatory factor in tumour growth. *Nat Rev Cancer* 2(1):38–47.
27. Jiang Y, et al. (2003) Gene expression profiling in a renal cell carcinoma cell line: Dissecting VHL and hypoxia-dependent pathways. *Mol Cancer Res* 1(6):453–462.
28. Dranoff G (2004) Cytokines in cancer pathogenesis and cancer therapy. *Nat Rev Cancer* 4(1):11–22.
29. Danielsson F, et al. (2013) Majority of differentially expressed genes are down-regulated during malignant transformation in a four-stage model. *Proc Natl Acad Sci USA* 110(17):6853–6858.
30. Jonasch E, et al. (2012) State of the science: an update on renal cell carcinoma. *Mol Cancer Res* 10(7):859–880.
31. Cheong H, Lu C, Lindsten T, Thompson CB (2012) Therapeutic targets in cancer cell metabolism and autophagy. *Nat Biotechnol* 30(7):671–678.
32. Robitaille AM, et al. (2013) Quantitative phosphoproteomics reveal mTORC1 activates de novo pyrimidine synthesis. *Science* 339(6125):1320–1323.
33. Ben-Sahra I, Howell JJ, Asara JM, Manning BD (2013) Stimulation of de novo pyrimidine synthesis by growth signaling through mTOR and S6K1. *Science* 339(6125):1323–1328.
34. Gerlinger M, et al. (2012) Intratumor heterogeneity and branched evolution revealed by multiregion sequencing. *N Engl J Med* 366(10):883–892.
35. Singh RB, Amare Kadam PS (2011) Investigation of tumor suppressor genes apart from VHL on 3p by deletion mapping in sporadic clear cell renal cell carcinoma (cRCC). *Urol Oncol* 31(7):1333–1342.
36. Brinckmann A, et al. (2002) Interferon-alpha resistance in renal carcinoma cells is associated with defective induction of signal transducer and activator of transcription 1 which can be restored by a supernatant of phorbol 12-myristate 13-acetate stimulated peripheral blood mononuclear cells. *Br J Cancer* 86(3):449–455.
37. Zambelli F, Prazzoli GM, Pesole G, Pavesi G (2012) Cscan: Finding common regulators of a set of genes by using a collection of genome-wide ChIP-seq datasets. *Nucleic Acids Res* 40(Web Server issue):W510–W515.
38. Agren R, et al. (2013) The RAVEN toolbox and its use for generating a genome-scale metabolic model for *Penicillium chrysogenum*. *PLOS Comput Biol* 9(3): e1002980.
39. Pique-Regi R, Cáceres A, González JR (2010) R-Gada: A fast and flexible pipeline for copy number analysis in association studies. *BMC Bioinformatics* 11:380.